

## Critical disorder and critical magnetic field of the nonequilibrium athermal random-field Ising model in thin systems

Svetislav Mijatović<sup>1</sup>,<sup>✉</sup> Dragutin Jovković,<sup>2,\*</sup> Sanja Janičević,<sup>3,\*</sup> and Djordje Spasojević<sup>1</sup>

<sup>1</sup>Faculty of Physics, University of Belgrade, POB 44, 11001 Belgrade, Serbia

<sup>2</sup>Faculty of Mining and Geology, University of Belgrade, POB 162, 11000 Belgrade, Serbia

<sup>3</sup>Faculty of Science, University of Kragujevac, POB 60, 34000 Kragujevac, Serbia



(Received 22 May 2019; revised manuscript received 17 July 2019; published 9 September 2019)

In the present study of the nonequilibrium athermal random-field Ising model we focus on the behavior of the critical disorder  $R_c(l)$  and the critical magnetic field  $H_c(l)$  under different boundary conditions when the system thickness  $l$  varies. We propose expressions for  $R_c(l)$  and  $H_c(l)$  as well as for the effective critical disorder  $R_c^{\text{eff}}(l, L)$  and effective critical magnetic field  $H_c^{\text{eff}}(l, L)$  playing the role of the effective critical parameters for the  $L \times L \times l$  lattices of finite lateral size  $L$ . We support these expressions by the scaling collapses of the magnetization and susceptibility curves obtained in extensive simulations. The collapses are achieved with the two-dimensional (2D) exponents for  $l$  below some characteristic value, providing thus a numerical evidence that the thin systems exhibit a 2D-like criticality which should be relevant for the experimental analyses of thin ferromagnetic samples.

DOI: [10.1103/PhysRevE.100.032113](https://doi.org/10.1103/PhysRevE.100.032113)

### I. INTRODUCTION

Study of nonequilibrium model systems with an avalanche-like response to external perturbations has been one of the most prominent issues in statistical physics during the last few decades [1–3]. This is because such response lies in the root of many of natural phenomena (e.g., earthquakes [4], motion of domain walls in ferromagnetic materials [5], neuronal activities in brain [6,7], and avalanches in wood samples treated under mechanical pressure [8]), making the studies of the related models of great practical as well as conceptual importance. One such model is the random-field Ising model (RFIM), which was extensively studied in a variety of its versions [9–12]. Thus, in the equilibrium version of the model recent progress offered some important answers on the universality principles [13,14], dimensional reduction [15], and supersymmetry [16]. In this paper a particular focus is on the nonequilibrium athermal (NEA) version that enables studies of the evolution in time of the spin systems that are not affected by the thermal fluctuations and are slowly driven by the external magnetic field through its nonequilibrium states.

Former theoretical and/or numerical studies of the NEA RFIM were dominantly performed on the spin systems situated on the equilateral cubic lattices in which case it was shown that the model exhibits a nontrivial critical behavior in dimensions  $2 \leq d \leq 5$  [17–21] and the mean-field criticality for  $d \geq 6$  [22–25]. Recently this limitation in scope has been lifted due to a growing scientific and technological interest regarding the behavior of thin systems. Physics of magnetism was not an exception because many experiments were performed on thin systems (e.g., ribbons and films) with one

dimension (thickness) significantly smaller than the other two [26–32].

So far, the RFIM in thin systems was studied in very few papers mainly on the grounds of an equilibrium model [33–37]. One exception is the study of nonequilateral systems [38], where it was shown how the critical disorder of the systems having finite thickness and infinite lateral sides changes with thickness on the crossover from three-dimensional (3D) to two-dimensional (2D) case, as well as how the effective critical disorder of finite systems behaves when the thickness and/or lateral sizes of these systems change. To continue this work, in this paper we study how the critical field of the systems with infinite base and finite thickness, and the effective critical field of finite nonequilateral systems, changes when the size of the system varies.

A well-known result regarding the model behavior on equilateral lattices is that it becomes independent of the choice of boundary conditions in the thermodynamic limit (i.e., when the system size increases to infinity), since the percentage of the spins affected by the different boundary conditions decays [39,40]. This, however, ceases to be true in the case of systems having finite thickness (and infinite lateral sides), because in the case of finite thickness the same percentage of spins is affected by the change of boundary conditions no matter how big the other two dimensions are. In this paper we show that the differences caused by the two most important types of boundary conditions imposed on finite nonequilateral systems (i.e., open or closed along thickness and closed in the remaining two directions) are retained in the thermodynamic limit, and that these differences become more and more pronounced as the systems get thinner and thinner so the fraction of the spins affected by the choice becomes large.

The paper is organized as follows: the model is described in the Sec. II, whereas the main results (theoretical

\*Also at the Faculty of Physics, University of Belgrade, POB 44, 11001 Belgrade, Serbia.

predictions and the numerical results regarding the effective critical disorder and the effective critical field) are given in Sec. III. Collapses of the magnetization and susceptibility curves are presented in Sec. IV, overall discussion in Sec. V, and conclusions in Sec. VI.

## II. MODEL

In the athermal nonequilibrium random-field Ising model studied in this paper, ferromagnetically coupled classical Ising spins  $S_i$  (i.e., spins that can take only the values  $+1$  or  $-1$ ) are located at a 3D cubic lattice having sizes  $(L, L, l)$  along the  $(x, y, z)$  directions, respectively, with thickness  $l \leq L$ . As the thermal fluctuations are neglected, spins interact only magnetically. Each spin  $S_i$  interacts with the external homogeneous magnetic field  $H$  having energy  $-HS_i$  in this field. Next, each  $S_i$  is ferromagnetically coupled via exchange interaction  $-J_{ij}S_iS_j$  with all of its nearest neighbors  $S_j$  and, in the simplest case (e.g., the case presented here), the exchange coupling constant is the same for each pair of nearest neighbors,  $J_{ij} = J$ . Finally, in (all versions of) the RFIM it is taken that there is a local magnetic field  $h_i$  at each lattice site  $i$  giving additional coupling  $-h_iS_i$  of  $S_i$  with  $h_i$ . For all the foregoing reasons, the Hamiltonian of the system reads

$$\mathcal{H} = -J \sum_{(i,j)} S_i S_j - H \sum_i S_i - \sum_i h_i S_i, \quad (1)$$

where the summation  $\sum_{(i,j)}$  runs over all distinct pairs of nearest neighboring spins. Regarding the local field, it varies randomly from site to site taking the values from some zero-centered distribution. In this paper it is the Gaussian distribution

$$\rho(h) = \frac{1}{\sqrt{2\pi}R} \exp\left(-\frac{h^2}{2R^2}\right), \quad (2)$$

and its standard deviation  $R$  is called *disorder* as it measures the amount of disorder in the system. From this distribution the values of the local field are chosen not only randomly but also independently at different sites, implying that  $\langle h_i \rangle = 0$  and  $\langle h_i h_j \rangle = R^2 \delta_{ij}$ , where  $\langle \cdot \rangle$  denotes averaging over all possible local field configurations  $\{h_i\}_{i=1}^N$  taken at  $N = L \times L \times l$  sites in the system, and  $\delta_{ij}$  is the standard Kronecker function. Furthermore, in the athermal version, each configuration of the local field is *quenched* (i.e., frozen), meaning that it is not altered throughout the system's evolution in time.

Unlike in the *equilibrium* version [41] (in which the system traverses solely throughout the equilibrium states corresponding to a given sequence of values taken by the external magnetic field  $H$ ), in the nonequilibrium version of the model the evolution of the system in time proceeds following the local relaxation rule stating that the spin  $S_i$  is stable as long as its sign is the same as the sign of the *effective field*

$$h_i^{\text{eff}} = J \sum_{(j)} S_j + H + h_i \quad (3)$$

at its site. The rule implies that all spins that are unstable at the moment  $t$  will flip at the next moment  $t + 1$  of discrete time and therefore affect their neighbors. Those of neighbors that become unstable will flip in the next next moment of time, and in this way an avalanche of spin flipping is created lasting as long as there are unstable spins in the system.

Once the system becomes stable the only way to create new avalanches is to drive the system by changing the external magnetic field. Here one can distinguish between different possible driving regimes, like the finite-driving regime [42–48], in which the external field is incremented by a fixed amount in each new moment of time, and the quasistatic regime in which the external field is kept constant during any avalanche and afterwards incremented by a fixed amount until creation of new avalanche(s). The zero-limit case of both of these regimes is the *adiabatic* regime, studied in this paper. In this regime, the external field is, like in the quasistatic regime, kept constant during the ongoing avalanche and afterwards changed not infinitely slowly but, for the increased efficiency, in a single step so as to flip exactly the least-stable spin, permitting in this way only a single avalanche at a time.

Finally, to fully describe the model, one has to specify the boundary conditions as well as the initial and final conditions. The boundary conditions are described and discussed in the next section, while as initial conditions we use  $H = -\infty$  and all  $S_i = -1$  (for other possible initial conditions see Refs. [47,49,50]). Then the external field is adiabatically increased until all spins become  $S_i = 1$ , meaning that our simulations are done along the rising branch of the hysteresis loop. To such a choice of initial and driving conditions, we have limited ourselves in this paper because they are mostly analyzed in the past and therefore have to be first studied in the initial phase of research of the current topic while the studies under different initial conditions and/or driving regimes are left for the future series of studies.

In our study we take  $J = 1$  and for each chosen value of disorder  $R$  we performed many simulations, each for a different configuration  $\{h_i\}_{i=1}^N$  of the random field. In every simulation we registered the sequence of the external magnetic field values flipping the (next) least stable spin and recorded the subsequent avalanche as a time sequence of the number  $n_t$  of spins flipped at the moment  $t$  (running from  $t = 0$  at the avalanche start up to  $t = T$  at the avalanche end). We used the data thus obtained to form the distributions of avalanche parameters *averaged* over all employed configurations of the random field corresponding to the chosen value of disorder.

The data presented in this paper correspond to the systems containing from  $256 \times 256 \times 2 = 131\,072$  to  $8192 \times 8192 \times 64 \approx 4.3$  billion spins and are obtained in simulations using the sorted list algorithm detailed in Ref. [51]. This algorithm efficiently finds the next most unstable spin and the value of the external field flipping that spin once the avalanche is over. In this way the simulation time per single run was greatly reduced, which enabled a large number of runs (from 200 for the largest up to 64 000 for the smallest systems) necessary to collect reliable statistics.

## III. EFFECTIVE CRITICAL PARAMETERS

The athermal RFIM is characterized by the three critical parameters, namely, the critical disorder  $R_c$ , the critical field  $H_c$ , and the critical magnetization  $M_c$ , so that the infinite RFIM spin systems behave as ferromagnets for disorders  $R < R_c$  and as paramagnets for  $R > R_c$  [18,20]. In the paramagnetic phase the magnetization curve  $M_R(H)$  is a smooth function of the external field  $H$ , whereas in the

ferromagnetic phase this curve is also smooth except at some transition value  $H_j(R)$  of the external field at which the system experiences a first-order phase transition manifested in a jump of magnetization  $\Delta M(R)$  that is caused by infinite avalanche(s). Both  $H_j(R)$  and  $\Delta M(R)$  depend on disorder  $R$ , and, when  $R$  tends to  $R_c$  from below, the transition field  $H_j(R)$  tends to  $H_c$ , while the magnetization jumps decrease to zero, giving the critical magnetization curve  $M_{R_c}(H)$ , which is a smooth function of  $H$  everywhere except at the critical field  $H_c$  where its first derivative  $dM/dH$  is infinite. The critical parameters  $R_c$ ,  $H_c$ , and  $M_c \equiv M_{R_c}(H_c)$  are nonuniversal, i.e., their values depend on the dimension  $d$  of the system and on the type of lattice at which the spins are situated [18,52,53]. Furthermore, different types of interactions may either move the model to different [54–56], or leave it in the same [57], universality class.

The foregoing behavior of infinite systems is to a certain extent also exhibited by the finite systems, but with some important differences. Thus, the role of the infinite avalanches is taken by the spanning avalanches, i.e., the large avalanches that span the finite system along at least one of its directions [19,58]. These avalanches are likely to appear at low and be absent at high disorders. The low- and high-disorder regions are separated by a narrow transition region of disorder in which the average number of spanning avalanches per single run gradually decreases from 1 to 0 when  $R$  increases. The center of this transition region is taken as an *effective critical disorder*  $R_c^{\text{eff}}$ . Its values depend on the type and size of the underlying lattice and in the thermodynamic limit (i.e., when the lattice of the given type becomes infinite) tend from above to the critical disorder  $R_c$ ; in the same limit the width of the transition region of disorder tends to zero [58].

Next, let us name as the *spanning field* each value  $H_{\text{sp}}$  of external field triggering a spanning avalanche at finite lattice [58]. For each value of disorder at the chosen lattice type, there is not a single value of  $H_{\text{sp}}$ , but instead a disorder-dependent distribution of its values concentrated in a rather narrow region of  $H$ . At the mode  $H_c^{\text{eff}}(R)$  of this distribution the susceptibility  $\chi = dM_R/dH$  of the magnetization curve  $M_R(H)$ , averaged over the random-field configurations with disorder  $R$ , has its maximum. So one could rightly call  $H_c^{\text{eff}} \equiv H_c^{\text{eff}}(R_c^{\text{eff}})$  (i.e., the value of this mode taken at the effective critical disorder  $R_c^{\text{eff}}$ ) as the *effective critical field* for the finite lattice of the chosen type because in finite systems it is the closest analog of the critical field  $H_c$  obtained in the thermodynamic limit for this lattice type.

In this paper we study the RFIM spin systems located at 3D cubic lattices of type  $L \times L \times l$  having the thickness  $l \leq L$ , where  $L$  is the (larger) linear size of the lattice along the remaining two lateral dimensions; the effective critical disorder and the effective critical field for such lattices we denote by  $R_c^{\text{eff}}(l, L)$  and  $H_c^{\text{eff}}(l, L)$ , respectively. In the thermodynamic limit, obtained when  $L \rightarrow \infty$  and constant  $l$ , these lattices promote a family of infinite 3D cubic lattices of different (finite) thickness  $l$ . For each  $l$ , the infinite RFIM spin system, located at such a lattice, exhibits a critical behavior described by the critical disorder

$$R_c(l) = \lim_{L \rightarrow \infty} R_c^{\text{eff}}(l, L), \quad (4)$$

the critical field

$$H_c(l) = \lim_{L \rightarrow \infty} H_c^{\text{eff}}(l, L), \quad (5)$$

and the critical magnetization

$$M_c(l) = \lim_{L \rightarrow \infty} M_c^{\text{eff}}(l, L), \quad (6)$$

together with the corresponding set of critical exponents having the values that may also vary with the thickness  $l$ ; see Ref. [59] for the variation of the effective exponents (e.g., the size exponent  $\tau$ ), which is of considerable importance for the analysis of thin ferromagnets experimental data.

On the course towards the thermodynamic limit the aspect ratio  $l/L$  of the  $L \times L \times l$  lattices decreases to zero because the thickness  $l$  is kept constant and the lateral size  $L$  increases to infinity. In a consequence, it is likely that even the avalanches of the linear size comparable to  $l$  span the system along its thickness (say,  $z$ ) direction. Therefore, it turned out to be appropriate to consider the avalanche as a spanning one if it spans the system along at least one of its lateral (say,  $x$  and  $y$ ) directions and to take into account only such spanning avalanches in the determination of the effective critical parameters for the  $L \times L \times l$  lattices.

At this point, the choice of the boundary conditions becomes relevant. Quite generally, one may consider the periodic (i.e., closed) or nonperiodic (i.e., open) boundary condition along any of the lattice directions. In the case of equilateral (i.e.,  $L \times L \times L$ ) cubic lattices the thermodynamic limit is not affected by any combination of such conditions taken along the  $x$ ,  $y$ , and  $z$  directions; however, the approach to the limit is the fastest if the all-boundary conditions are closed (CCC). For this reason it seems natural to choose the CCO boundary conditions, i.e., the conditions that are closed along both of the lateral directions and open along the thickness for a better correspondence to the physical boundaries of the system. With such a choice, a method for determining the effective critical disorder  $R_c^{\text{eff}}(l, L)$ , together with its limits  $R_c(l)$  and the crossover behavior from the 3D to 2D systems, is introduced in Ref. [38]. Nevertheless, at least because of conceptual reasons, it seems meaningful to expand the study from CCO also to CCC boundary conditions.

In what follows we expand the previous study [38] of the effective disorder  $R_c^{\text{eff}}(l, L)$  from the CCO to the CCC case and reveal the behavior of the effective critical field  $H_c^{\text{eff}}(l, L)$  for both types of boundary conditions. These findings enable us to establish the thermodynamic limits  $R_c(l)$  and  $H_c(l)$  of the effective critical disorder or field and to investigate their crossovers from the equilateral 3D to the 2D model realized by thinning out the thickness  $l$ . Regarding the third critical parameter,  $M_c(l)$ , we mention that the determination of its value is rather difficult (e.g., in the equilateral 3D case it is indicated only in the caption of Fig. 1 in Ref. [18]) and therefore left for further studies.

#### A. Effective critical disorder for the CCC boundary conditions

As in the case of CCO boundary conditions, the distribution  $N(R; l, L)$  of the number of spanning avalanches triggered per single run on the  $L \times L \times l$  cubic lattice with CCC boundary conditions can be reasonably well approximated by the

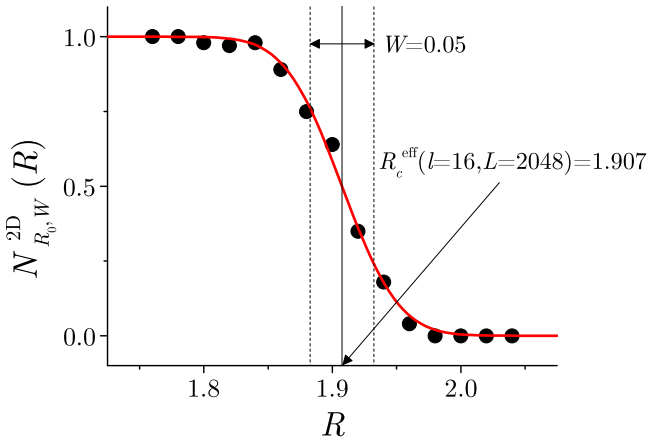


FIG. 1. Example of obtaining  $R_c^{\text{eff},C}(l, L)$  in the case of the CCC boundary conditions on the cubic lattice with  $l = 16$  and  $L = 2048$ .

model function

$$N_{R_0, W}(R) = 0.5 \times \text{erfc}[(R - R_0)/W]; \quad (7)$$

cf. Fig. 1. Here  $\text{erfc}(v) \equiv (2/\sqrt{\pi}) \int_v^\infty e^{-t^2} dt$  is the complementary error function of  $v = (R - R_0)/W$  with the inflection point centered at  $R = R_0$  and the width  $W$  of the transition region of disorder, i.e., the region of  $R$  in which  $\text{erfc}(v)$  falls from (roughly)  $3/4$  to (roughly)  $1/4$ . For a constant thickness  $l$ , the estimated values of both parameters  $R_0$  and  $W$  depend on the lateral lattice size  $L$  so that when  $L$  increases they monotonically decrease:  $W$  to zero and  $R_0$  to its  $L \rightarrow \infty$  limit. Furthermore, as  $R_0$  separates the region of disorders in which the presence of the spanning avalanches is more likely than their absence, we take it, like in the CCO boundary conditions case, as our estimate for the effective critical disorder  $R_c^{\text{eff},C}(l, L)$  on the  $L \times L \times l$  cubic lattices

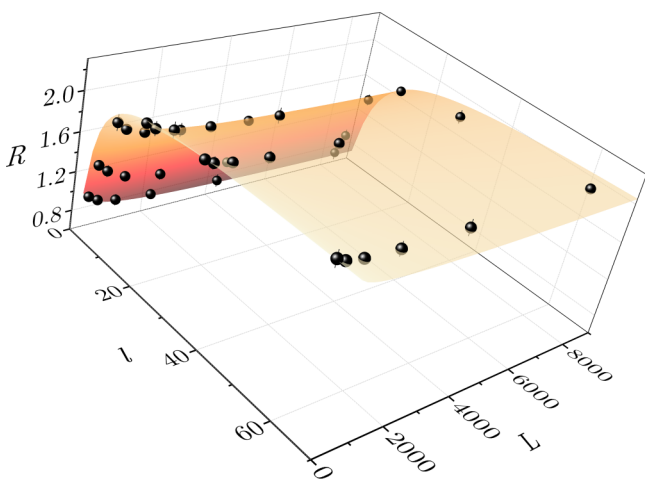


FIG. 2. Symbols present our numerical data for the effective critical disorder  $R_c^{\text{eff},C}(l, L)$  in the CCC case (i.e., the closed boundary conditions imposed in all three directions of the  $L \times L \times l$  cubic lattice). The data are shown against the system thickness  $l$  and lateral linear size  $L$  together with the surface (10) that fits the  $R_c^{\text{eff},C}(l, L)$  data with 0.07 maximum residual for  $l \geq 8$  and 0.21 for  $l = 4$  when  $A' = 1.17 \pm 0.22$  and  $v' = 6.29 \pm 0.17$ ; see Fig. 9 and Discussion.

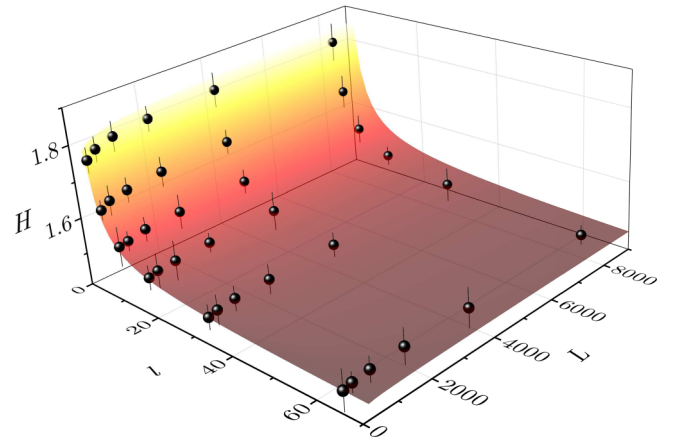


FIG. 3. Numerical data for the effective critical field  $H_c^{\text{eff},O}(l, L)$  in the CCO case (i.e., boundary conditions that are closed in two lateral directions and open in the thickness direction of the  $L \times L \times l$  cubic lattice). The numerical data, presented by dots, are shown against the system thickness  $l$  and lateral linear size  $L$  together with the theoretical surface (15) that best fits the  $H_c^{\text{eff},O}(l, L)$  data for  $B = 0.20 \pm 0.07$  with 0.01 maximum residual for all of the employed thicknesses; see Fig. 9 and Discussion.

with CCC boundary conditions. Consequently, we take the limits  $R_c^C(l) = \lim_{L \rightarrow \infty} R_c^{\text{eff},C}(l, L)$  as the critical disorders for the infinite cubic lattices of thickness  $l$  with a closed boundary condition along their thickness.

Formally speaking, the values of the effective critical disorder  $R_c^{\text{eff},C}(l, L)$ , taken as a function of two discrete quantities  $l$  and  $L$ , may be viewed as the points lying at a surface in a 3D space with coordinates  $(l, L, R)$ . In order to predict the shape of this surface we have started from the following two hypotheses:

$$\frac{R_c^C(l) - R_c^{3D}}{R_c^C(l)} = \frac{\Delta}{l^{1/\nu_{3D}}} \quad (8)$$

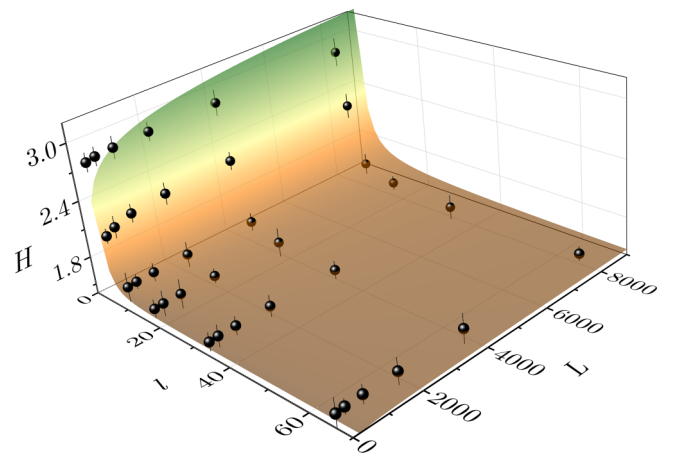


FIG. 4. The same as in Fig. 3, but for the effective critical field  $H_c^{\text{eff},C}(l, L)$ , and the theoretical prediction (19) with constant  $B' = 2.32 \pm 0.19$  in the CCC case. Here the maximum residual is 0.09 for  $l \geq 8$  and 0.8 for  $l = 4$ ; see Fig. 9 and Discussion.

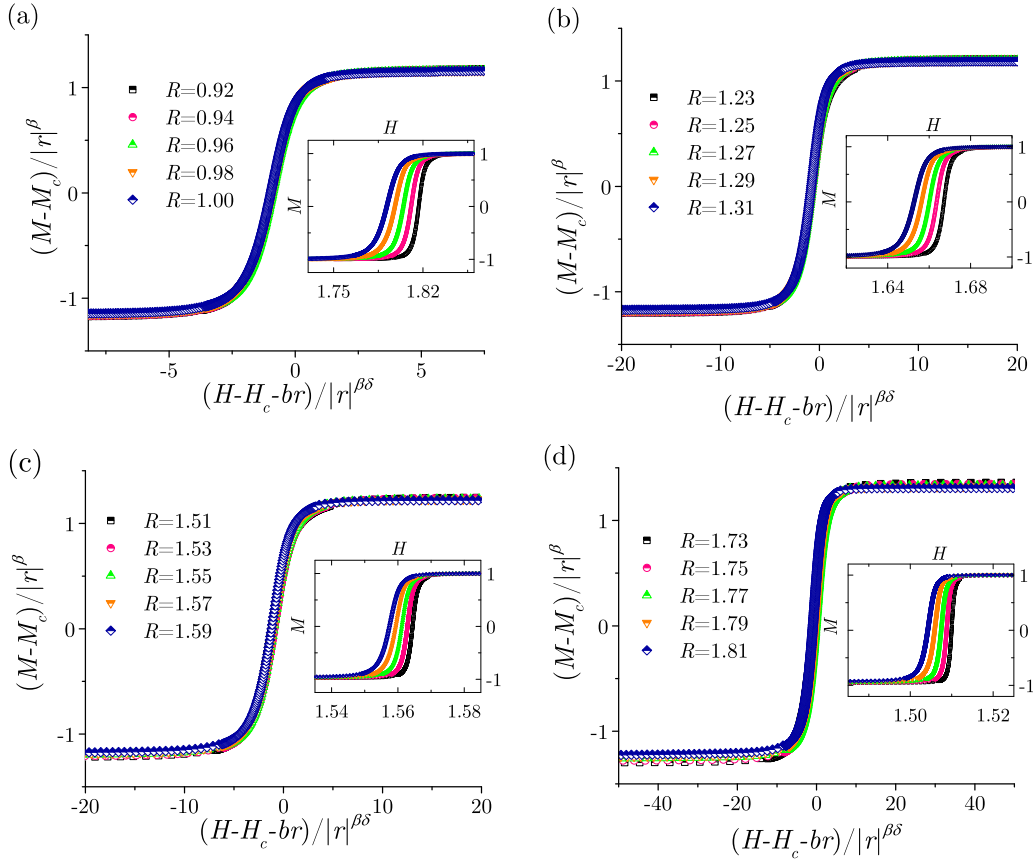


FIG. 5. Scaling collapses in the CCO case of the magnetization curves shown in insets. The collapses are achieved using the values from the 2D model for the critical exponents, and the magnetization curves are obtained for different disorders given in the legends for systems with thicknesses (a)  $l = 2$ , (b)  $l = 4$ , (c)  $l = 8$ , and (d)  $l = 16$ . Note that for the sake of simpler notation we omitted  $l$  in  $H_c(l)$  and  $r(l)$  in the titles of the axes of the abscissa.

and

$$\frac{R_c^{\text{eff,C}}(l, L) - R_c^{\text{C}}(l)}{R_c^{\text{eff,C}}(l, L)} = \frac{(A' - \Delta)l^{1/\nu'}}{(l^{1/\nu_{3D}} - \Delta)L^{1/\nu'}}, \quad (9)$$

which are both supported by the results of our simulations and qualitatively justified in Appendix A. The first one, hypothesis (8), is the same as hypothesis (10) in Ref. [38], so  $R_c^{3D} = 2.16$  is the critical disorder for the *ordinary* 3D RFIM [3] (i.e., the model situated at the cubic lattice that is infinite along all three directions),  $\Delta \equiv 1 - R_c^{3D}/R_c^{2D} \approx -3$  where  $R_c^{2D} = 0.54$  is the critical disorder for the ordinary 2D model on the infinite quadratic lattice [20,21], and  $\nu_{3D}$  is the correlation length exponent describing the divergence  $\xi \sim r^{-\nu_{3D}}$  of the correlation length  $\xi$  with the reduced disorder  $r = (R - R_c^{3D})/R$  in the proximity of the critical point of the ordinary 3D model.

The second hypothesis, hypothesis (9), is a modified hypothesis (11) from Ref. [38] as it contains a *new* exponent  $\nu'$  (instead of  $\nu_{2D}$ ) and a different constant  $A'$  in the expression

$$A'(l) \equiv \frac{(A' - \Delta)l^{1/\nu'}}{l^{1/\nu_{3D}} - \Delta}$$

for the amplitude  $A'(l)$  in the CCC case reflecting the differences in avalanche propagation caused by the different boundary conditions. Thus, while the avalanches are halted at each of the open system boundaries in the CCO case (so

the large avalanches are sandwiched between these boundaries and effectively propagate as 2D avalanches), there are no boundary limits for the avalanche propagation in the CCC case, causing larger values of the effective critical disorder, which becomes more and more pronounced as the lattice thickness decreases.

Following the same procedure as in Ref. [38], and taking into account the two special cases  $l = 2$  and  $l = L$ , we derive the theoretical prediction

$$R_c^{\text{th,C}}(l, L) = R_c^{3D} \left[ 1 - \frac{\Delta}{l^{1/\nu_{3D}}} - \frac{(A' - \Delta)l^{1/\nu'}}{L^{1/\nu'}l^{1/\nu_{3D}}} \right]^{-1} \quad (10)$$

for the shape of the surface on which should lie the values of the effective critical disorder for the RFIM spin systems situated at the cubic lattices of type  $L \times L \times l$  with closed boundary conditions along all directions.

In Fig. 2 we show the theoretical surface (10) with  $A' = 1.17 \pm 0.22$  and  $\nu' = 6.29 \pm 0.17$  giving the best fit of our  $R_c^{\text{eff,C}}(l, L)$  data. These, as well as the all other data presented in this paper, are gathered in simulations of 36 different systems of type  $L \times L \times l$ , where  $l$  ranges from 2 to 64 and  $L$  from 256 to 8192. To this end we ran 200 simulations for 15 different values of disorders ranging from below to above the effective critical disorder  $R_c^{\text{eff,C}}(l, L)$  for each of the employed  $L \times L \times l$  systems. *Thus, 3000 runs were needed to get each*

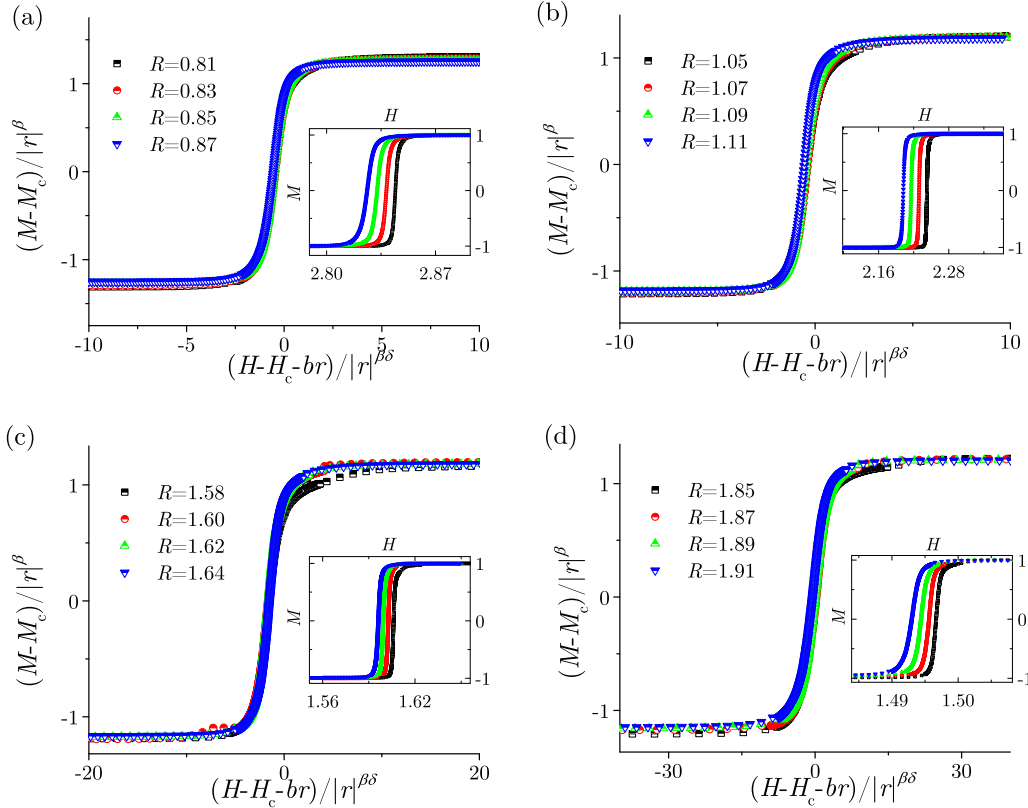


FIG. 6. The same as in Fig. 5, but for the CCC case.

of the presented  $R_c^{\text{eff},C}(l, L)$  values, giving in total  $36 \times 3000$  runs to obtain Fig. 2. One run time lasted from few seconds for smaller systems up to half a day for larger systems. That means that every single point in Fig. 1 was extracted from 200 runs with independent and different random-field configurations, and then  $R_c^{\text{eff}}(l, L)$  was obtained by fitting the points to the complementary error function using the maximum likelihood method. That method gives the error estimation as well, and the error bars are presented by the vertical lines in Fig. 2. For  $l \geq 8$  the theoretical surface fits the points within their error bars, and the maximum deviation of one point from the surface is 0.07. However, for  $l < 8$  the deviations are bigger, which is shown in Fig. 9 and there discussed.

### B. Effective critical field

The effective critical field (i.e., the value of the external field maximizing the susceptibility of a finite system at the effective critical disorder) depends on the boundary conditions imposed on the adiabatic NEA RFIM spin systems located at the  $L \times L \times l$  cubic lattices. For this reason one has to distinguish between  $H_c^{\text{eff},O}(l, L)$  and  $H_c^{\text{eff},C}(l, L)$ , i.e., between the effective critical field in the CCO and CCC cases, and analogously between their thermodynamic limits  $H_c^O(l) = \lim_{L \rightarrow \infty} H_c^{\text{eff},O}(l, L)$  and  $H_c^C(l) = \lim_{L \rightarrow \infty} H_c^{\text{eff},C}(l, L)$ , which, unlike the critical disorders, turned out to be different.

Following the findings regarding the behavior of the effective critical field in the 2D model on quadratic lattices [21,58],

here we propose that in the CCO case

$$H_c^{\text{eff},O}(l, L) - H_c^O(l) = \frac{B(l)}{L^{1/\nu_{2D}}}, \quad (11)$$

since it is expected that avalanches propagate similar to the avalanches in the pure 2D model when the thickness  $l$  is fixed; for more explanation of (11) see Appendix B. Here the amplitude  $B(l)$  is yet-to-be-determined function of thickness  $l$ , and  $\nu_{2D}$  is the correlation length exponent in the 2D model. Furthermore, as for  $l \geq 2$  the critical field of infinite systems of thickness  $l$  monotonically decreases when  $l$  increases, and we expect that avalanches in those systems behave like avalanches in equilateral 3D systems, we also propose that, like some other critical parameters in both equilibrium and nonequilibrium versions of the model [35,38],  $H_c^O(l)$  has a power law approach

$$H_c^O(l) - H_c^{3D} = \Theta l^{-1/\nu_{3D}} \quad (12)$$

to the 3D limit  $H_c^{3D}$ . The approach is specified by the constant  $\Theta = 2^{1/\nu_{3D}} [H_c^O(2) - H_c^{3D}]$  stemming from (12) for the limiting thickness  $l = 2$  [59,60]. Such a small thickness allowed simulations of the systems with a very large base; henceforth we obtained  $H_c^O(2) = 1.85 \pm 0.01$  and calculated  $\Theta = 0.68 \pm 0.07$  using the known values  $H_c^{3D} = 1.435$  and  $\nu_{3D} = 1.41$  from the 3D model on equilateral lattices [18].

Equations (11) and (12) enabled us to advance to the expression

$$H_c^{\text{eff},O}(l, L) - H_c^{3D} = \frac{\Theta}{l^{1/\nu_{3D}}} + \frac{B(l)}{L^{1/\nu_{2D}}}, \quad (13)$$

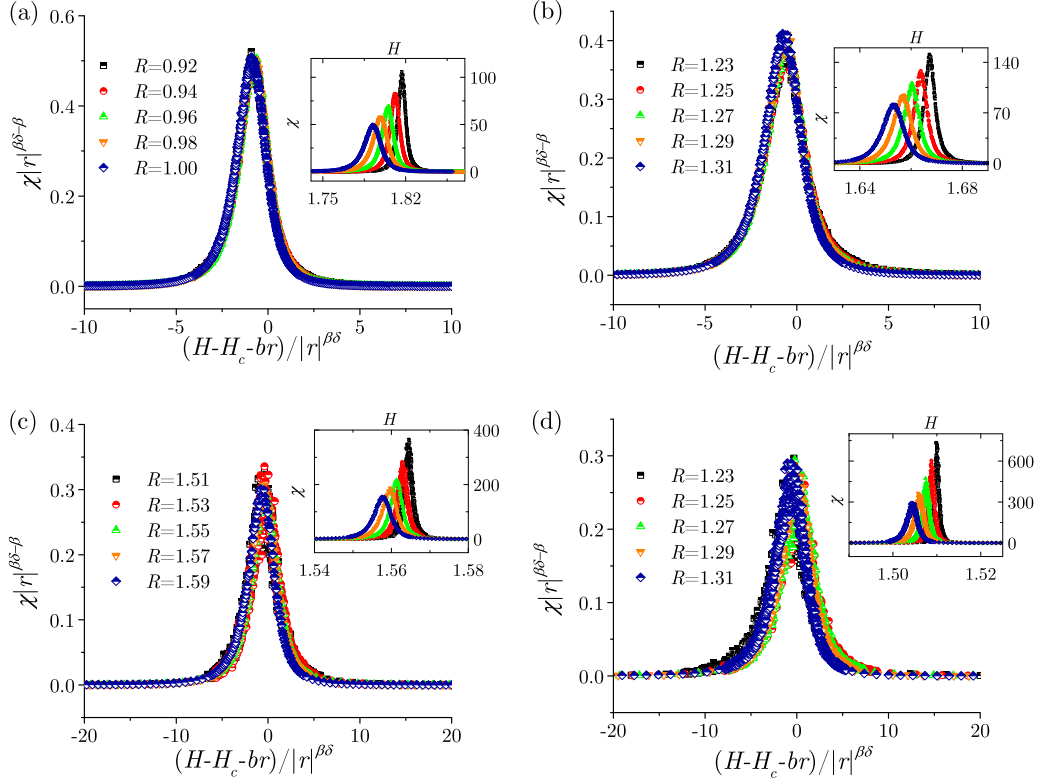


FIG. 7. The same as in Fig. 5, but for the susceptibility curves in the CCO case.

containing the unknown amplitude  $B(l)$ . In order to find it we employed that  $H_c^{\text{eff},O}(L) - H_c^{3D} = B/L^{1/v_{3D}}$  in the CCO 3D model on equilateral lattices (analogously to the 2D model in Ref. [21]), which is in fact a special case of (13) realized for  $l = L$ . This gave us

$$\frac{B}{l^{1/v_{3D}}} = \frac{\Theta}{l^{1/v_{3D}}} + \frac{B(l)}{l^{1/v_{3D}}},$$

implying that

$$B(l) = \frac{B - \Theta}{l^{1/v_{3D}}} l^{1/v_{2D}}, \quad (14)$$

which eventually led us to the analytic form of our theoretical prediction

$$H_c^{\text{th},O}(l, L) = H_c^{3D} + \frac{\Theta}{l^{1/v_{3D}}} + \frac{B - \Theta}{l^{1/v_{3D}}} \left(\frac{l}{L}\right)^{1/v_{2D}}, \quad (15)$$

for the effective critical field  $H_c^{\text{eff},O}(l, L)$  taken as function of  $l$  and  $L$ . The comparison of our numerical data for  $H_c^{\text{eff},O}(l, L)$  and prediction (15) with  $B = 0.20 \pm 0.07$ , giving the best fit of the  $H_c^{\text{eff},O}(l, L)$  data by the theoretical prediction (15), is presented in Fig. 3.

Analogously, in the CCC case we found that, instead of (12), the expression

$$H_c^C(l) - H_c^{3D} = \Theta' l^{-1/v_{3D}} \quad (16)$$

for the critical field  $H_c^C(l)$  of infinite systems with thickness  $l$  holds, containing a *different* constant  $\Theta'$ . Its value  $\Theta' = 2.32$  was calculated from the value  $H_c^C(2) \approx 2.85$  of the critical field of infinite systems of thickness  $l = 2$  obtained on the

grounds of extensive simulations on these lattices with a very large base. Similarly, instead of (11), we found the expression

$$H_c^{\text{eff},C}(l, L) - H_c^C(l) = \frac{B'(l)}{L^{1/v'}}, \quad (17)$$

which holds for the effective critical field  $H_c^{\text{eff},C}(l, L)$  with the same critical exponent  $v'$  as in (10), and the amplitude

$$B'(l) = \frac{B' - \Theta'}{l^{1/v_{3D}}} l^{1/v'}. \quad (18)$$

This eventually led us to our theoretical prediction

$$H_c^{\text{th},C}(l, L) = H_c^{3D} + \frac{\Theta'}{l^{1/v_{3D}}} + \frac{B' - \Theta'}{l^{1/v_{3D}}} \left(\frac{l}{L}\right)^{1/v'}, \quad (19)$$

which is compared in Fig. 4 with our numerical  $H_c^{\text{eff},C}(l, L)$  data using the value  $B' = 2.32 \pm 0.19$ , which gives the best fit under the CCC boundary conditions.

For both CCO and CCC cases and for each disorder  $R = R_c^{\text{eff}}(l, L)$ , the value  $H_c^{\text{eff}}(l, L)$  of the external field at which the susceptibility has its maximum is determined from the susceptibility curve obtained by averaging a large number (ranging from 200 for the largest up to 32 000 for the smallest systems) of individual susceptibility curves that correspond to different random-field configurations, which was necessary because at  $R = R_c^{\text{eff}}(l, L)$  the spanning avalanches appear. For each  $l$  and  $L$  the error bar was estimated as the greatest deviation from  $H_c^{\text{eff}}(l, L)$  of the value of external field at which some spanning avalanche occurred, and such error bars of  $H_c^{\text{eff}}(l, L)$  are presented as vertical lines in Figs. 3 and 4. In the CCO case, i.e., Fig. 3, the agreement between the

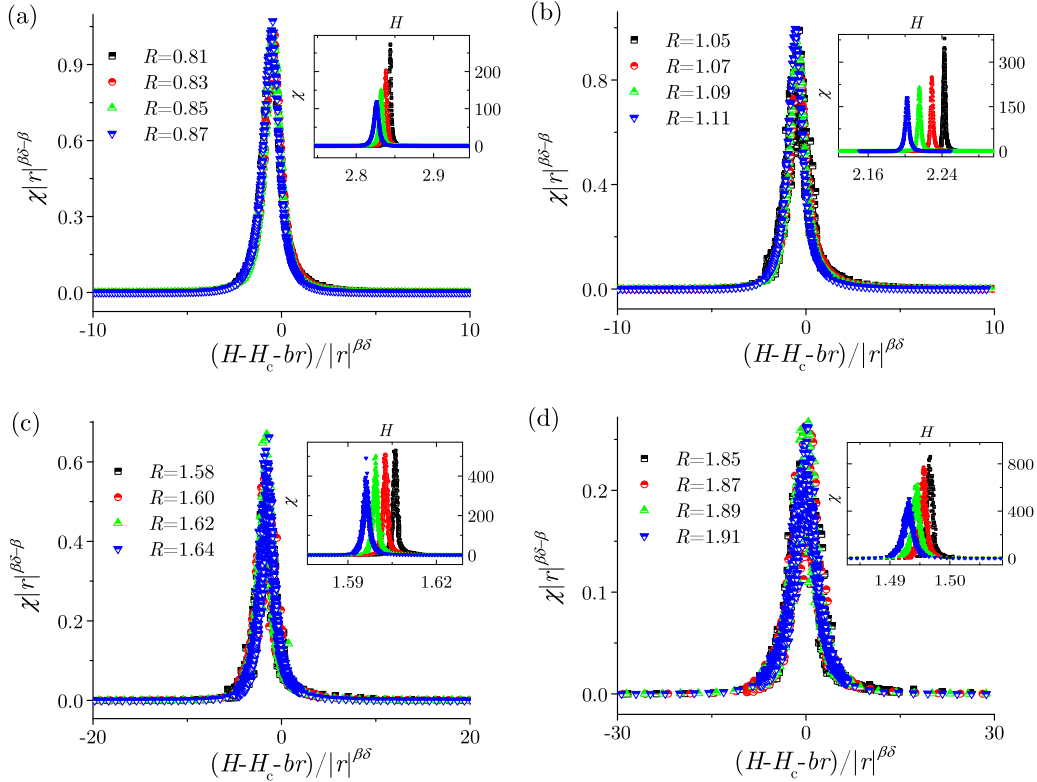


FIG. 8. The same as in Fig. 7, but for the susceptibility curves in the CCC case.

theoretical surface and the numerically extracted values lies in the range  $\pm 0.01$  for all values of  $l$  and  $L$ . The situation is different in the CCC case, where the agreement is in the range  $\pm 0.09$  for  $l \geq 8$ , which is satisfactory, but for  $l < 8$  some huge deviations appear, which is again, as in the case of effective critical disorder, explained in detail in the caption of Fig. 9.

#### IV. SCALING OF MAGNETIZATION AND SUSCEPTIBILITY CURVES

The theoretical prediction (7) from Ref. [38] and the analogous prediction (8) from this paper lead in the  $L \rightarrow \infty$  limit to the same prediction,

$$R_c^{\text{th}}(l) = R_c^{3D} \left[ 1 - \frac{\Delta}{l^{1/\nu_{3D}}} \right]^{-1}, \quad (20)$$

for the critical disorder of infinite systems with thickness  $l$  in both the CCO and CCC boundary conditions, whereas (12) and (16) lead to the predictions for the critical fields

$$H_c^{\text{th},O}(l) = H_c^{3D} + \frac{\Theta}{l^{1/\nu_{3D}}}, \quad (21)$$

$$H_c^{\text{th},C}(l) = H_c^{3D} + \frac{\Theta'}{l^{1/\nu_{3D}}}, \quad (22)$$

which are affected by the choice of boundary conditions due to different values of constants  $\Theta$  and  $\Theta'$ . All three of them can be tested by attempting to collapse the magnetization and susceptibility curves using the values they predict for the critical disorder and critical field.

#### A. Scaling of magnetization curves

For a chosen infinite RFIM spin system, its magnetization  $M_R(H)$  scales in a vicinity of the critical point  $(R_c, H_c, M_c)$  for that system as [3,18]

$$m_R(H) = |r|^\beta \mathcal{M}_\pm(h'/|r|^{\beta\delta}), \quad (23)$$

where  $m_R(H) = M_R(H) - M_c$  is the reduced magnetization,  $r = (R - R_c)/R$  is the reduced disorder,  $h' = H - H_c + br$  is the reduced magnetic field rotated by the parameter  $b$ , and  $\mathcal{M}_\pm(x)$  denotes a pair of universal scaling functions depending on the single variable  $x = h'/|r|^{\beta\delta}$  in the range of disorder above (+) and below (−) the critical disorder  $R_c$ , respectively; for more explanation of (23) see Appendix C. The scaling of variables in (23) is described by the two critical exponents:  $\beta$  (describing the scaling  $\Delta M \sim |r|^\beta$  of the magnetization jump below  $R_c$ ) and  $\delta$  (describing the scaling  $m \sim h'^\delta$  of the reduced magnetization with the reduced magnetic field at the critical disorder).

In *thin* systems with *open* boundary conditions along the  $z$  axis (i.e., CCO case), even relatively small avalanches easily reach the system's borders along thickness and afterwards propagate along the remaining two directions effectively as 2D avalanches [59]. So, in this case, one can expect that the exponents  $\beta$  and  $\delta$  have the values as in the 2D model on equilateral lattices ( $\beta = 0.15$ ,  $\delta = 32$  [20]) and test whether the values of  $R_c^{\text{th}}(l)$  and  $H_c^{\text{th},O}(l)$ , predicted by (20) and (21), can play the role of  $R_c$  and  $H_c$ . The results of such test, shown in Fig. 5 for the thicknesses  $l = 2, 4, 8, 16$  and lateral size  $L = 8192$ , suggest that the foregoing assumptions are fulfilled.

On the other hand, in the case of *thin* systems with *closed* boundary conditions in all directions (i.e., the CCC case) where the propagation of avalanches is not affected by the system borders, the situation is different. Thus, in the case of the thinnest (i.e.,  $l = 2$  and  $l = 4$ ) systems the values of  $R_c^{\text{th}}(l)$  and  $H_c^{\text{th,C}}(l)$ , predicted by (20) and (22), cannot play the role of  $R_c$  and  $H_c$ , and the values of exponents different from the 2D ones need to be used; cf. Fig. 6(a) and 6(b) and see the discussion in the next section. Conversely, for the moderately thick (i.e.,  $l = 8$  and  $l = 16$ ) systems, one can use the 2D values of exponents  $\beta$  and  $\delta$  together with the values predicted by (20) and (22) for  $R_c$  and  $H_c$ ; see Figs. 6(c) and 6(d).

Finally, for the systems with thickness  $l > 16$ , the collapses with the 2D values of exponents  $\beta$  and  $\delta$  cannot be achieved in a satisfying manner because the thicker the system the less it resembles the 2D. Thus, in order to perform a satisfying collapse for the thicker systems with a finite base, the values of the exponents  $\beta$  and  $\delta$  need to be altered towards their values for the 3D model on equilateral lattices. More detailed analysis of the flow of the exponents' values is given in Ref. [59].

### B. Scaling of susceptibility curves

By differentiating (23) with respect to the external field  $H$  we obtain the scaling law of the susceptibility curves  $\chi_R(H) \equiv dM_R(H)/dH$  as

$$\chi_R(H) = |r|^{\beta-\beta\delta} \mathcal{M}'_{\pm}(h'/|r|^{\beta\delta}), \quad (24)$$

where  $\mathcal{M}'_{\pm} = \mathcal{M}_{\pm}(x)/dx$  are the universal scaling functions for the susceptibility curves above and below  $R_c$ ; see Refs. [3,18]. The collapses are shown in Fig. 7 (CCO case) and Fig. 8 (CCC case) and are achieved in the same way as the corresponding collapses of magnetization, shown in Figs. 5 and 6, respectively.

## V. DISCUSSION

In this paper we have analyzed how the change of boundary conditions affects the behavior of the NEA RFIM of spin systems with finite thickness; for the influence of other factors (like preexisting domains and/or interfaces) see, for instance, Refs. [50,61,62]. Thus, we found that besides the differences in the CCO and CCC cases regarding the values of exponents  $\beta$  and  $\delta$ , and our theoretical predictions for the critical field of infinite systems, a significant difference between the numerical values for the effective critical disorders  $R_c^{\text{eff,O}}(l, L)$  and  $R_c^{\text{eff,C}}(l, L)$  is also encountered in the case of very thin systems.

In Fig. 9 we present the proposed theoretical curves for infinite systems of thickness  $l$ : curve (20) for the critical disorder  $R_c(l)$  in the main part of Fig. 9(a) and curves (21) and (22) for the critical field  $H_c^{\text{th,O}}(l)$  and  $H_c^{\text{th,C}}(l)$  in the CCO and CCC cases, respectively, in the main part of Fig. 9(b). In addition, the theoretical curves (7) from Ref. [38] and (10) from this paper are calculated for a set of fixed values of  $L$  and varying  $l$  and presented by lines in the inset of Fig. 9(a), together with two numerical data sets (symbols) for the effective critical disorder in the CCO and CCC cases. In order to adequately capture these markedly different data sets exponents denoted

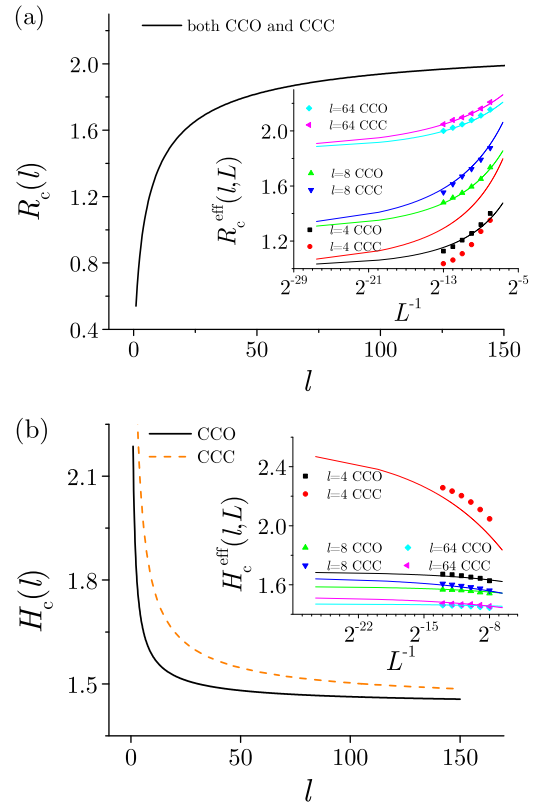


FIG. 9. (a) Main: theoretical curve (20) giving the (same) prediction for the critical disorder in both the CCO and CCC cases. Inset: numerical values (dots) of the effective critical disorder shown against the lateral size  $L$  for the systems of fixed thicknesses, and the corresponding curves representing the theoretical predictions (7) from Ref. [38] and (10) from this paper for the CCO and the CCC cases, respectively. (b) Main: theoretical curve for the critical field given by (21) for the CCO and by (21) for the CCC case. Inset: the same as for the inset in panel (a) but for the effective critical field.

to  $L$  in (7) from Ref. [38] and (10) from this paper must be different,  $\nu' \neq \nu_{2D}$  (which was expected since avalanche spreading along  $x$  and  $y$  dimensions significantly differs in the CCC and CCO cases).

Similarly, in the inset of Fig. 9(b), the curves (15) and (19) are shown together with points representing the corresponding numerical data of the effective critical field. From this, it can be noticed that the numerical data in the CCO case, as well as in the CCC case for  $l \geq 8$ , agree with the theoretical predictions, but *not* in the CCC case for  $l = 4$ .

In our opinion, the reason for the above discrepancies is as follows: because flipping of a spin  $s_i$ , located at the (say) top border, affects the effective field  $h_j^{\text{eff}}$  (3) of all of its nearest neighbors, and because there are more of such neighbors if this boundary is closed, the spreading of the avalanches reaching top (or bottom) border is facilitated which causes a noticeable lowering of the effective critical field if the fraction of such spins is significant. Therefore, the  $l \geq 8$  systems behave similarly because at most 25% of the spins are affected by the change of boundary conditions from the CCO to the CCC case, whereas the  $l \leq 4$  systems

behave differently owing to a quite high percentage of the spins affected by that change (50% for  $l = 4$  and 100% for  $l = 2$ ). This in turn causes the departure of numerical data for the effective critical field  $R_c^{\text{eff},C}(l, L)$  of the  $l \leq 4$  systems in the CCC case from the simple theoretical prediction (10) treating all the spanning avalanches as effectively 2D. And, as in this case the effective critical field  $H_c^{\text{eff},C}(l, L)$  (i.e., the field that maximizes susceptibility) is determined at the (lower than theoretically predicted) numerical value  $R_c^{\text{eff},O}(l, L)$  of effective critical disorder, its numerical values for  $l \leq 4$  systems lie above the theoretical prediction (19); cf. the inset in Fig. 9(b).

Finally, let us point out that our predictions (10), (15), and (19), together with (20), (21), and (22), give only the leading terms in the scaling with  $l$  (and  $L$ ) of the corresponding quantities. Correction terms in their forms are to be expected (see Appendix B), leading to smaller deviations of the theoretical predictions from the numerical results, and this will be a subject of our future studies. This also applies to the variables  $r$  and  $h'$  approximating the correct scaling variables in the ordinary 3D model.

## VI. CONCLUSION

In this paper we have studied the effective critical disorder  $R_c^{\text{eff}}(l, L)$  and the effective critical field  $H_c^{\text{eff}}(l, L)$  for the nonequilibrium athermal random-field Ising model situated on the  $L \times L \times l$  cubic lattices together with their thermodynamic limits, the critical disorder  $R_c(l)$  and the critical field  $H_c(l)$ , pertaining to the lattices of infinite lateral size  $L$  and finite thickness  $l$ . We have proposed the theoretical predictions for all of these quantities and supported the predictions for finite lattices by the numerical data obtained in extensive simulations. The analysis is performed using periodic (i.e., closed) boundary conditions in both lateral directions and two types (closed and open) along thickness, the latter one better corresponding to the experimental situations.

We found that for bigger thicknesses there are no significant differences caused by these two types of conditions, whereas for thin systems the differences appear together with some anomalous behavior in the limit of very small  $l$ . The differences are manifested in the scaling collapses of the magnetization and susceptibility curves that are well described by the values of critical exponents for the 2D model in the open boundary case for all  $l \geq 2$ , but not for  $l < 8$  in the case of closed conditions.

In our final conclusion, we consider that our study provides strong numerical evidence that the considered model on the family of cubic lattices of finite thickness exhibits a criticality that is for thin systems with the open boundaries along thickness described by the critical exponents from the 2D model, which should be relevant for the analyses of experimental data obtained on thin ferromagnetic samples.

## ACKNOWLEDGMENT

This work was supported by the Ministry of Education, Science and Technological Development of Republic of Serbia under project 171027.

## APPENDIX A: QUALITATIVE JUSTIFICATION OF SCALING HYPOTHESES (8) AND (9)

Let us start from the statement that the correlation length becomes of the order of system size,  $\xi \sim l$ , when disorder approaches the effective critical disorder for the finite system of size  $l$ . Specially, in equilateral 3D systems of size  $l$ , this means that  $1 - R_c^{3D}/R_c^{\text{eff}}(l, L = l) \sim l^{-1/\nu_{3D}}$  when disorder tends to critical,  $R \rightarrow R_c^{\text{eff}}(l, L = l)$ ; as evidence for analogous statement in the case of the equilateral 2D RFIM systems see (10) and Fig. 6 in Ref. [20].

Now, as  $R_c^C(l)$  behaves similarly to  $R_c^{\text{eff}}(l, L = l)$  for sufficiently big  $l$ , one may conjecture that

$$\frac{R_c^C(l) - R_c^{3D}}{R_c^C(l)} = \frac{\Delta'}{l^{1/\nu_{3D}}} \quad (\text{A1})$$

holds for the RFIM systems with finite thickness with CCC boundary conditions like the analogous hypothesis (10) from Ref. [38] in the CCO case [an alternative way of justifying (A1)]: systems of size  $L \times L \times l$ , where  $L \gg l$  with changing  $l$  and  $L$  are 3D systems whose critical disorders approach  $R_c^{3D}$  in a 3D manner. On the other hand those systems behave effectively as systems of infinite base and thickness  $l$ , leading to (A1).

Nevertheless, some differences between the cases are to be expected. Namely, when the boundaries are open along thickness, then in  $l > 1$  systems the avalanches are halted at the system boundaries and therefore, being squeezed between the boundaries, propagate in a 2D manner as is shown in Ref. [59], making the transition from  $l = 2$  to  $l = 1$  smooth. However, in the CCC case, the avalanches in the  $l > 1$  systems can propagate along thickness, which causes them to behave differently than in the  $l = 1$  case. Therefore, the transition from  $l = 2$  to  $l = 1$  is not smooth in the CCC case, and the lower value of  $l$  for which (A1) is suitable is  $l = 2$ . Since  $l = 2$  is a small thickness, it allowed us to simulate the systems with large bases and thereupon find that  $\Delta' = 2^{1/\nu_{3D}}[R_c^C(2) - R_c^{3D}]/R_c^C(2) \approx -3.02$ . On the other hand, as for the CCO case  $\Delta = 1 - R_c^{3D}/R_c^{2D} \approx -3$  one may take that

$$\Delta' = \Delta$$

within the error bars, promoting (A1) into hypothesis (8), which is the same as hypothesis (10) in Ref. [38].

Regarding the hypothesis (9), let us start from the equation

$$\frac{R_c^{\text{eff},C}(l, L) - R_c^{3D}}{R_c^{\text{eff},C}(l, L)} = \frac{R_c^{\text{eff},C}(l, L) - R_c^C(l)}{R_c^{\text{eff},C}(l, L)} + \frac{R_c^C(l) - R_c^{3D}}{R_c^C(l)} \frac{R_c^C(l)}{R_c^{\text{eff},C}(l, L)}, \quad (\text{A2})$$

which for  $L = l$  becomes

$$\frac{R_c^{\text{eff},C}(l, l) - R_c^{3D}}{R_c^{\text{eff},C}(l, l)} = \frac{R_c^{\text{eff},C}(l, l) - R_c^C(l)}{R_c^{\text{eff},C}(l, l)} + \frac{R_c^C(l) - R_c^{3D}}{R_c^C(l)} \frac{R_c^C(l)}{R_c^{\text{eff},C}(l, l)}. \quad (\text{A3})$$

The left-hand side of (A3) describes the approach of the effective critical disorder  $R_c^{\text{eff},C}(l, l)$  to the critical disorder  $R_c^{3D}$  for the equilateral systems of size  $l$  in the ordinary 3D

RFIM, so

$$\frac{R_c^{\text{eff.C}}(l, l) - R_c^{3D}}{R_c^{\text{eff.C}}(l, l)} = \frac{A'}{l^{1/\nu_{3D}}}, \quad (\text{A4})$$

where the amplitude  $A'$  characterizes the approach in the CCC case. Next, our numerical data for  $l > 8$  suggest for the first term on the right-hand side of (A3) that

$$\frac{R_c^{\text{eff.C}}(l, L) - R_c^C(l)}{R_c^{\text{eff.C}}(l, L)} = \frac{A'(l)}{L^{1/\nu'}}, \quad (\text{A5})$$

i.e., that the approach of  $R_c^{\text{eff.C}}(l, L)$  to  $R_c^C(l)$  when the lateral size  $L$  diverges is of a power law type specified by the exponent  $\nu'$ ; see the inset in Fig. 9. Now, after replacing in (A3) the left-hand sides of (A4) and (A5) by the matching right-hand sides, one can solve (A3) for  $A'(l)$  and, in this way, find that

$$A'(l) = \frac{(A' - \Delta)l^{1/\nu'}}{l^{1/\nu_{3D}} - \Delta}. \quad (\text{A6})$$

This equation led us to hypothesis (9), which is a modified hypothesis (11) from Ref. [38] as it contains a different constant  $A'$  and exponent  $\nu'$  that is, according to our numerical data, different from the correlation length exponent  $\nu_{2D}$  in the ordinary 2D model.

#### APPENDIX B: THE APPROACH OF THE EFFECTIVE CRITICAL FIELD TO THE CRITICAL FIELD WHEN THE SYSTEM SIZE DIVERGES

Generally the choice of the scaling variables specifying the displacement of a system from its critical point is not unique. The simplest choice of such variables in the case of equilateral RFIM systems of size  $L$  is  $\{R - R_c, H - H_c, 1/L\}$ ; however, any other triple of variables  $\{x_1, x_2, x_3\}$  having a smooth 1-1 correspondence with that simplest triple and vanishing at the critical point  $\{R_c, H_c, 0\}$  can equally serve as well. Nevertheless, not all such choices are equally suitable. As elaborated in Ref. [63] only proper (i.e., correct) choices enable exact scaling manifested in the existence of universal scaling functions that are generalized homogeneous functions depending in the foregoing RFIM case not on three, but on two, scaled variables.

As the form of the correct RFIM scaling variables is not known, different approximations have been proposed so far. Thus,  $r \equiv (R - R_c)/R$ ,  $h' \equiv H - H_c + br$ , and  $1/L$  was proposed by Sethna *et al.* (see Ref. [3] and the references therein), whereas Perez-Reche and Vives [63] proposed  $u = u_1 + Au_1^2$  and  $v = v_1 + B'u_1$  instead of  $r$  and  $h'$ , where  $u_1 = (R - R_c)/R_c$  and  $v_1 = (H - H_c)/H_c$ . Although seemingly different, these two choices should lead to essentially the same collapses because in the near proximity of the critical point  $r = u_1 - u_1^2 + u_1^3 + \dots$  and so on, implying that  $r \approx u$  and  $h' \approx v$ .

From the functional point of view, the role of the scaling variable measuring the deviation of the external field  $H$  from its critical value  $H_c$  should be that it, *inter alia*, enables collapsing of the susceptibility curves. For this reason, such a variable should be centered at the effective critical field  $H_c^{\text{eff}}(R, L)$ , i.e., the value of  $H$  at which the susceptibility

curve, obtained at disorder  $R$  for the equilateral RFIM system of size  $L$ , attains its maximum. However, the form of  $H_c^{\text{eff}}(R, L)$  is not known, and both  $H_c - br$  in Ref. [3] and  $H_c(1 - B'u_1)$ , i.e., (30) in Ref. [63], are in fact two similar first-order approximations of unknown  $H_c^{\text{eff}}(R, L)$ , expressed in terms of deviations  $r$  and  $u_1$  from  $R_c$ , respectively.

Despite  $r$  and  $u_1$  being not the same variables, their values  $r_c^{\text{eff}}(L) \equiv [R_c^{\text{eff}}(L) - R_c]/R_c^{\text{eff}}(L)$  and  $u_{1c}^{\text{eff}} \equiv [R_c^{\text{eff}}(L) - R_c]/R_c$ , attained at the effective critical disorder  $R_c^{\text{eff}}(L)$  for the equilateral RFIM systems of size  $L$ , both approach zero when  $L \rightarrow \infty$  following power laws,  $\sim L^{-\nu}$ , specified by the same exponent  $\nu$  (and differing in the corresponding correction terms). On these grounds, one can propose hypotheses (11) and (12) in the CCO case, and hypotheses (16) and (17) in the CCC case of  $L \times L \times l$  3D RFIM systems.

In Eq. (10) from Ref. [63] the deviation of external field from the critical external field was considered:

$$\langle H \rangle_\alpha - H_c \sim -C_\alpha L^{-1/\mu},$$

where  $\langle H \rangle_\alpha$  stands for the average of the external field values triggering the  $\alpha$ -type of spanning avalanches. By comparing this equation to Eqs. (16) and (17) one can notice the difference in critical exponents ( $\mu = \nu/\beta\delta$ ), from which may arise question whether Eqs. (16) and (17) are correct. Let us note that previous equation [Eq. (10) from Ref. [63]] holds for  $R = R_c$ , i.e., for  $u_1 = 0$ , whereas  $H_c^{\text{eff}}(R, L)$  corresponds to  $R = R_c^{\text{eff}}(L)$ , i.e., to  $u_{1c}^{\text{eff}} > 0$ . So Eq. (29) from Ref. [63] gives that

$$\begin{aligned} \langle H \rangle_\alpha (R_c^{\text{eff}}(L), L) - H_c &= -H_c B' u_{1c}^{\text{eff}} - \frac{\hat{h}_\alpha (u_{1c}^{\text{eff}} L^{1/\nu})}{L^{1/\mu}} \\ &\sim -H_c B' \frac{D}{L^{1/\nu}} - \frac{\hat{h}_\alpha(D)}{L^{1/\mu}}, \end{aligned}$$

where  $u_{1c}^{\text{eff}}$  corresponds to given  $L$  and therefore  $u_{1c}^{\text{eff}} L^{1/\nu} \approx D$ , where  $D$  is a constant independent of  $L$ . Because  $1/\nu < 1/\mu$ , this implies that the leading term for big  $L$  is proportional to  $L^{-1/\nu}$ , which leads us again to hypotheses (11), (12), (16), and (17).

#### APPENDIX C: COLLAPSING OF MAGNETIZATION CURVES

Equation (23) follows from the statement (substantiated by the corresponding renormalization group analysis, e.g., in Ref. [22]) that sufficiently close to the critical point the singular part of the Gibbs free energy per degree of freedom [i.e., the part giving divergent (some or all of the) response functions at the critical point] is a generalized homogeneous function

$$g(a^{\alpha_1} x_1, a^{\alpha_2} x_2, a^{\alpha_3} x_3, \dots) = ag(x_1, x_2, x_3, \dots),$$

of its (scaling) variables  $x_1, x_2, x_3, \dots$  measuring the distance to the critical point; here  $a > 0$  is a renormalization step, and  $\alpha_1, \alpha_2, \alpha_3, \dots$  are appropriate exponents. In the case of infinite RFIM systems and  $x_1 = r$ ,  $x_2 = h'$  this implies that the reduced magnetization  $m = -\partial g / \partial h'$  satisfies

$$m(r, h') = a^{-1+\alpha_2} m(a^{\alpha_1} r, a^{\alpha_2} h'),$$

or equivalently

$$m(r, h') = |r|^{(1-\alpha_2)/\alpha_1} \mathcal{M}_\pm(|h'|^{-\alpha_2/\alpha_1}),$$

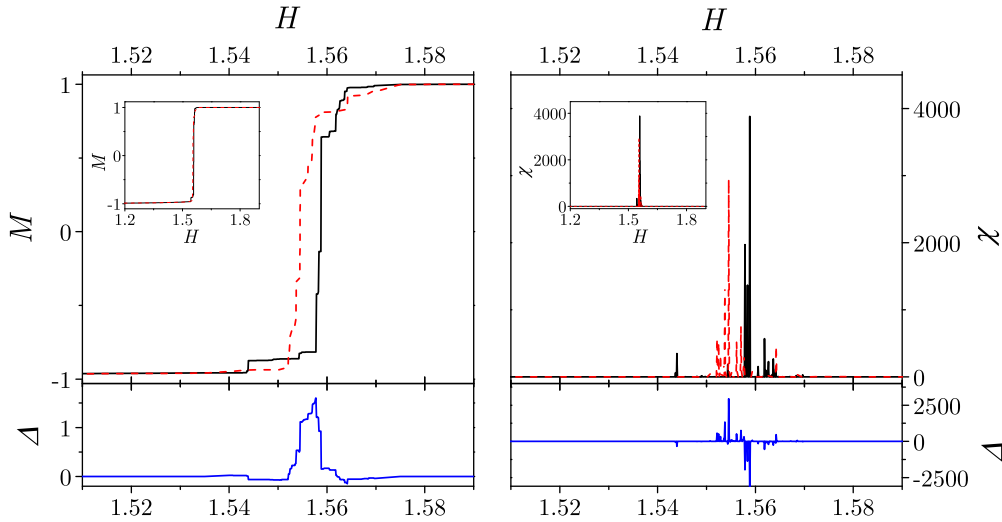


FIG. 10. Fluctuations between the magnetization curves (left) and the susceptibility curves (right) corresponding to two different samples both at the effective critical disorder for  $L = 1024$  and  $l = 8$ . The individual curves are shown in the upper parts of both panels (using the finer or coarser  $H$  scale in the main parts or insets), whereas their differences  $\Delta$  (dashed-solid) are shown in the lower parts.

when the renormalization step is taken as  $a = |r|^{-1/\alpha_1}$  and  $\mathcal{M}_{\pm}(h'|r|^{-\alpha_2/\alpha_1}) \equiv m(\pm 1, h')$ , which equals (23) with  $(1 - \alpha_2)/\alpha_1 = \beta$  and  $\alpha_2/\alpha_1 = \beta\delta$ .

Regarding the scaling variables, here we follow the choice  $r = (R - R_c)/R$  and  $h' = H - H_c + br$  adopted by Sethna and collaborators who showed (see the review [3] and the references quoted therein) why in the expression for the reduced external magnetic field  $h'$  there should be a term proportional to  $r$ ; for other choices see Refs. [19,63].

In theoretical analyses and in presentations of numerical data the averaged magnetization and susceptibility curves are

used. These curves are obtained by averaging over (theoretically, all, and in simulations all employed) random-field samples giving individual curves that fluctuate from sample to sample. As we simulated the systems at their effective critical disorder, such fluctuations, illustrated in Fig. 10, prove to be large. Therefore, we used many samples to reduce statistical scattering in the averaged curves, and we estimated the maximum uncertainty of the effective critical field  $H_c^{\text{eff}}(l, L)$ , corresponding to the peak of the averaged susceptibility curve, as the maximum deviation between this value and the values taken by the spanning field, i.e., the field triggering some spanning avalanche.

- 
- [1] D. P. Belanger and T. Nattermann, in *Spin Glasses and Random Fields*, edited by A. P. Young (World Scientific, Singapore, 1998), p. 251.
- [2] J. P. Sethna, K. Dahmen, S. Kartha, J. A. Krumhansl, B. W. Roberts, and J. D. Shore, *Phys. Rev. Lett.* **70**, 3347 (1993).
- [3] J. P. Sethna, K. A. Dahmen, and O. Perković, in *The Science of Hysteresis*, edited by G. Bertotti and I. Mayergoyz (Academic, Amsterdam, 2006), p. 107.
- [4] J. Davidsen and M. Baiesi, *Phys. Rev. E* **94**, 022314 (2016).
- [5] A. Benassi and S. Zapperi, *Phys. Rev. B* **84**, 214441 (2011).
- [6] N. Friedman, S. Ito, B. A. W. Brinkman, M. Shimono, R. E. Lee DeVille, K. A. Dahmen, J. M. Beggs, and T. C. Butler, *Phys. Rev. Lett.* **108**, 208102 (2012).
- [7] C. Bedard, H. Kroger, and A. Destexhe, *Phys. Rev. Lett.* **97**, 118102 (2006).
- [8] T. Makinen, A. Miksic, M. Ovaska, and M. J. Alava, *Phys. Rev. Lett.* **115**, 055501 (2015).
- [9] K. A. Dahmen, J. P. Sethna, M. C. Kuntz, and O. Perković, *J. Magn. Magn. Mater.* **226–230**, 1287 (2001).
- [10] B. Tadić, *Phys. Rev. Lett.* **77**, 3843 (1996).
- [11] I. Balog, G. Tarjus, and M. Tissier, *Phys. Rev. B* **97**, 094204 (2018).
- [12] U. Schulz, J. Villain, E. Brézin, and H. Orland, *J. Stat. Phys.* **51**, 1 (1988).
- [13] N. G. Fytas and V. Martin-Mayor, *Phys. Rev. Lett.* **110**, 227201 (2013).
- [14] N. G. Fytas, V. Martin-Mayor, M. Picco, and N. Sourlas, *Phys. Rev. Lett.* **116**, 227201 (2016).
- [15] N. G. Fytas, V. Martin-Mayor, M. Picco, and N. Sourlas, *Phys. Rev. E* **95**, 042117 (2017).
- [16] N. G. Fytas, V. Martin-Mayor, G. Parisi, M. Picco, and N. Sourlas, *Phys. Rev. Lett.* **122**, 240603 (2019).
- [17] G. Grinstein, *J. Appl. Phys.* **55**, 2371 (1984).
- [18] O. Perković, K. A. Dahmen, and J. P. Sethna, *Phys. Rev. B* **59**, 6106 (1999).
- [19] F. J. Perez-Reche and E. Vives, *Phys. Rev. B* **67**, 134421 (2003).
- [20] Dj. Spasojević, S. Janičević, and M. Knežević, *Phys. Rev. Lett.* **106**, 175701 (2011).
- [21] Dj. Spasojević, S. Janičević, and M. Knežević, *Phys. Rev. E* **84**, 051119 (2011).
- [22] K. A. Dahmen and J. P. Sethna, *Phys. Rev. B* **53**, 14872 (1996).
- [23] O. Perković, K. A. Dahmen, and J. P. Sethna, [arXiv:cond-mat/9609072v1](https://arxiv.org/abs/cond-mat/9609072v1).

- [24] Dj. Spasojević, S. Janičević, and M. Knežević, *Europhys. Lett.* **76**, 912 (2006).
- [25] B. Ahrens and A. K. Hartmann, *Phys. Rev. B* **83**, 014205 (2011).
- [26] E. Puppini, *Phys. Rev. Lett.* **84**, 5415 (2000).
- [27] S. Yang and J. L. Erskine, *Phys. Rev. B* **72**, 064433 (2005).
- [28] K.-S. Ryu, H. Akinaga, and S.-Ch. Shin, *Nat. Phys.* **3**, 547 (2007).
- [29] K. Merazzo, D. Leitao, E. Jimenez, J. Araujo, J. Camarero, R. P. del Real, A. Asenjo, and M. Vazquez, *J. Phys. D* **44**, 505001 (2011).
- [30] H.-S. Lee, K. S. Ryu, C. Y. You, K. R. Jeon, S. Y. Yang, S. S. P. Parkin, and S. C. Shin, *J. Magn. Magn. Mater.* **325**, 13 (2013).
- [31] G. Z. dos Santos Lima, G. Corso, M. A. Correa, and R. L. Sommer, P. Ch. Ivanov, and F. Bohn, *Phys. Rev. E* **96**, 022159 (2017).
- [32] F. Bohn, G. Durin, M. A. Correa, N. Ribeiro Machado, R. Domingues Della Pace, C. Chesman, and R. L. Sommer, *Sci. Rep.* **8**, 11294 (2018).
- [33] L. L. Liu and H. E. Stanley, *Phys. Rev. Lett.* **29**, 927 (1972).
- [34] K. Binder, *Thin Solid Films* **20**, 367 (1974).
- [35] K. Kaneda, Y. Okabe, and M. Kikuchi, *J. Phys. A* **32**, 7263 (1999).
- [36] K. W. Lee and C. E. Lee, *Phys. Rev. B* **69**, 094428 (2004).
- [37] Y. Laosiritaworn, J. Poulter, and J. B. Staunton, *Phys. Rev. B* **70**, 104413 (2004).
- [38] Dj. Spasojević, S. Mijatović, V. Navas-Portella, and E. Vives, *Phys. Rev. E* **97**, 012109 (2018).
- [39] L. A. Nunes Amaral, A.-L. Barabasi, and H. E. Stanley, *Phys. Rev. Lett.* **73**, 62 (1994).
- [40] A. A. Middleton and D. S. Fisher, *Phys. Rev. B* **65**, 134411 (2002).
- [41] Y. Liu and K. A. Dahmen, *Europhys. Lett.* **86**, 56003 (2009); *Phys. Rev. E* **79**, 061124 (2009).
- [42] R. A. White and K. A. Dahmen, *Phys. Rev. Lett.* **91**, 085702 (2003).
- [43] B. Tadić, *Physica A* **270**, 125 (1999).
- [44] S. L. A. de Queiroz and M. Bahiana, *Phys. Rev. E* **64**, 066127 (2001).
- [45] F. J. Perez-Reche, B. Tadić, L. Mañosa, A. Planes, and E. Vives, *Phys. Rev. Lett.* **93**, 195701 (2004).
- [46] F. J. Perez-Reche, L. Truskinovsky, and G. Zanzotto, *Phys. Rev. Lett.* **101**, 230601 (2008).
- [47] N. J. Zhou, B. Zheng, and Y. Y. He, *Phys. Rev. B* **80**, 134425 (2009).
- [48] R. H. Dong, B. Zheng, and N. J. Zhou, *Europhys. Lett.* **98**, 36002 (2012).
- [49] L. Roters, A. Hucht, S. Lübeck, U. Nowak, and K. D. Usadel, *Phys. Rev. E* **60**, 5202 (1999).
- [50] S. K. Nandi, G. Biroli, and G. Tarjus, *Phys. Rev. Lett.* **116**, 145701 (2016).
- [51] M. C. Kuntz, O. Perkovic, K. A. Dahmen, B. W. Roberts, and J. P. Sethna, *Comput. Sci. Eng.* **1**, 73 (1999).
- [52] P. Shukla and D. Thongjaomayum, *J. Phys. A* **49**, 235001 (2016).
- [53] S. Janičević, S. Mijatović, and Dj. Spasojević, *Phys. Rev. E* **95**, 042131 (2017).
- [54] K. Kovacs and Z. Neda, *Phys. Lett. A* **361**, 18 (2007).
- [55] J. A. Perez-Benitez, J. Capo-Sanchez, and L. R. Padovese, *Comput. Mater. Sci.* **44**, 850 (2009).
- [56] J.-C. Angles d'Auriac, and F. Igloi, *Phys. Rev. E* **94**, 062126 (2016).
- [57] E. Vives and A. Planes, *J. Magn. Magn. Mater.* **221**, 164 (2000).
- [58] Dj. Spasojević, S. Janičević, and M. Knežević, *Phys. Rev. E* **89**, 012118 (2014).
- [59] B. Tadić, S. Mijatović, S. Janičević, Dj. Spasojević, and G. J. Rodgers, *Sci. Rep.* **9**, 6340 (2019).
- [60] The thickness  $l = 1$  corresponds to the 2D model having the smaller critical field  $H_c^{2D} = 1.275$  than  $H_c^O(2)$ , which probably comes from the significantly smaller coordination number ( $z_c = 4$  for  $l = 1$  and  $z_c \geq 5$  for  $l \geq 2$ ). This causes a nonmonotonic behavior of  $H_c^O(l)$  as a function of  $l$  and, therefore, (12) cannot be extended to the entire range of  $l$ .
- [61] V. Navas-Portella and E. Vives, *Phys. Rev. E* **93**, 022129 (2016).
- [62] B. Tadić, *Physica A* **493**, 330 (2018).
- [63] F. J. Perez-Reche and E. Vives, *Phys. Rev. B* **70**, 214422 (2004).